J. Electr. Electron. Mater.
Vol. 39, No. 1, pp. 79-87 January 2026
doi: https://doi.org/10.4313/JEEM.2026.39.1.10
ISSN 1226-7945(Print), 2288-3258(Online)

Early Stage Report : Graduate Research

Montmorillonite/rGO 복합체의 전기적 퍼콜레이션 거동을 통한 저항형 습도 센서의 감도 및 안정성 향상

유주형, 이승기

부산대학교 재료공학과

Enhanced Sensitivity and Stability of Resistive Humidity Sensors via Electrical Percolation Dynamics in Montmorillonite/rGO Composites

Ju Hyoeng Yu and Seoung-Ki Lee

School of Materials Science and Engineering, Pusan National University, Busan 46241, Republic of Korea

(Received November 11, 2025; Revised November 26, 2025; Accepted November 29, 2025)

Abstract: Humidity monitoring of exhaled breath has emerged as a vital approach for noninvasive respiratory health assessment, underscoring the need for sensitive and reliable humidity sensors. Despite its high conductivity and hydrophilic functional groups, reduced graphene oxide (rGO) often undergoes irreversible moisture adsorption and gradual oxidation by residual water, resulting in sensitivity degradation and long-term instability during cycling. In this study, a montmorillonite/reduced graphene oxide (MMT/rGO) composite is developed as a room-temperature humidity-sensing material, exhibiting an optimized response of 115%, more than 14 times higher than that of pristine rGO. This superior performance originates from the synergistic interaction between the reversible MMT swelling and the conductive rGO network near the electrical percolation transition, which ensures excellent stability and repeatability under repeated humidity cycles. These findings suggest that the MMT/rGO composite provides a cost-effective and biocompatible platform for next-generation wearable humidity sensors capable of continuous respiratory monitoring.

Keywords: Resistive humidity sensor, Montmorillonite, Reduced graphene oxide, Swelling, Electrical percolation transition, Solution based method

1. INTRODUCTION

Increasing attention to healthcare monitoring has heightened the demand for accurate and continuous respiratory diagnostics. By tracking human respiration, we can detect physiological abnormalities at an early stage, facilitating preventive healthcare and personalized medical management [1,2]. Because exhaled breath mainly consists of water vapor, along with trace gaseous components, real-time humidity monitoring serves as a reliable indirect indicator of respiratory patterns and potential health conditions. In this reason, humidity sensing has become a crucial technology for noninvasive respiratory diagnostics and wearable healthcare applications [3-6]. Various transduction mechanisms, including capacitive [7,8], surface acoustic wave (SAW) [9], quartz crystal microbalance (QCM) [10], optical [11,12], and resistive types

✉ **Seoung-Ki Lee; ifriend@pusan.ac.kr**

[3,6,13] have been explored for humidity detection. Among these, resistive-type humidity sensors have drawn particular attention due to their simple configuration, low power consumption, and compatibility with standard microelectromechanical system (MEMS) fabrication processes [14]. These characteristics enable device miniaturization, large-scale integration, and wireless operation, making them suitable for real-time respiratory monitoring systems. Conductive polymers and metal oxides have been widely investigated as sensing materials for resistive humidity sensors, but both materials have intrinsic limitations [15]. Conductive polymers have been studied for decades because of their light weight, simple fabrication, low-cost scalability, and mechanical flexibility. Despite these merits, their poor stability in high-humidity environments reduces their reliability and biocompatibility for humidity detection [15,16]. Metal oxide semiconductors provide an alternative approach that offers high sensitivity and fast response at room temperature. On the other hand, long-term stability issues of metal oxide such as drift and hysteresis under sustained humid conditions due to slow desorption and film limits their application in sustainable skin-interfaced devices [17]. These challenges demonstrate the need for new humidity-sensing materials with high stability, biocompatibility, and room-temperature operation. Graphene-based materials have emerged as promising candidates due to their large specific surface area, high carrier mobility, and low electronic noise, enabling rapid and stable responses under ambient conditions [18]. Among them, reduced graphene oxide (rGO) is particularly attractive for its high electrical conductivity and residual oxygen groups (–COOH, –OH) that enhance hydrophilicity and water adsorption. This combination of electrical sensitivity and surface reactivity makes rGO highly suitable for resistive humidity detection [19,20]. However, the strong hydrogen bonding between rGO and water molecules often leads to irreversible adsorption, and the residual moisture subsequently oxidizes the rGO surface, resulting in sensitivity degradation and long-term instability during cyclic operation [18]. These limitations indicate the need for complementary material that can facilitate reversible and reliable humidity sensing for respiratory monitoring.

Montmorillonite (MMT), a monoclinic layered clay mineral, readily intercalates water molecules between its layers, exhibiting up to seven-fold volumetric expansion upon hydration. Because of its strong moisture uptake capability, biocompatibility, and chemical safety, MMT is widely used in applications such as food packaging, pharmaceutical formulations, and cosmetic products [21,22]. Moreover, MMT exhibits highly reversible water adsorption–desorption behavior over repeated humidity cycles [23]. Building on these advantages, the integration of MMT into an rGO-based humidity-sensing platform establishes a complementary relationship between the two materials. rGO offers high electrical conductivity that enables efficient transduction of humidity-induced resistance changes, whereas MMT provides reversible water sorption, structural stability, and biocompatibility. Through this combined functionality, the composite is expected to improve long-term stability and enable the development of body-compatible humidity sensors.

In this study, we propose a MMT/rGO composite as a stable and biocompatible sensing material for humidity detection at room temperature. rGO flakes were uniformly mixed with MMT using a simple solution-based process, and the composition was optimized to maximize the humidity response. By utilizing the high stability, hydrophilicity, and natural abundance of MMT, the MMT/rGO composite provides a cost-effective and environmentally stable platform for wearable humidity sensors with reliable and continuous respiration-monitoring capabilities.

2. MATERIALS AND METHOD

2.1 Preparation of Montmorillonite/Graphene Composite

Graphene ink (0.4 wt% rGO flakes in IPA) was purchased from Chang Sung. MMT was purchased from Sigma-Aldrich. The solvent isopropyl alcohol (IPA) was also obtained from Sigma-Aldrich. A MMT suspension was prepared by dispersing MMT in IPA at a concentration of 52.63 wt%. The suspension was dispersed by sonication for 1 min to ensure uniform dispersion. The prepared MMT suspension was then mixed with graphene ink to form an MMT/rGO composite solution, followed by 1 min of additional sonication. The mixing volume ratio of the MMT suspension to the graphene ink was systematically varied to prepare composite solutions with ratios ranging from 0:10 to 7:3. Each composite was

designated according to its MMT fraction, and the corresponding wt% of MMT and rGO for each composite formulation is summarized in Table 1.

2.2 Fabrication of Montmorillonite/Graphene Composite–Based Humidity Sensor

A Cr (5 nm)/Au (50 nm) film was deposited on the cleaned glass substrates using a thermal evaporator under a chamber pressure of 8×10^{-6} Torr. Photoresist (AZ5214-E Photoresist, Sigma-Aldrich) patterning was performed using an aligner, followed by etching with Au etchant (KI, Sigma-Aldrich) and Cr etchant ($(NH_4)_2Ce(NO_3)_6 \cdot HNO_3$, Sigma-Aldrich) to define the interdigitated electrode (IDE) pattern. The resulting IDE structure featured a channel length of 0.1 mm and a channel width of 16.7 mm. The MMT/rGO composite solution was then spin-coated onto the IDE-deposited glass substrate at 500 rpm for 30s. The composite-coated substrates were baked at 80°C for 10 min to evaporate the residual solvent and enhance film adhesion.

2.3 Microstructural and Compositional Analysis

Surface morphology was examined using field-emission scanning electron microscopy (FE-SEM, TESCAN MIRA3) at an accelerating voltage of 20 kV. Prior to imaging, the samples were sputter-coated with a thin layer of gold to prevent charging and improve image clarity. Elemental composition analysis was conducted using energy-dispersive X-ray spectrometer (EDS) attached to the same SEM instrument operated at 20 kV.

2.4 Humidity Sensing Measurements

Humidity-sensing characteristics were evaluated in a microchamber (Nextron). Ar gas (5N) was used as the carrier gas. Relative humidity inside the chamber was controlled using a specially designed bubbler (Nextron). During each measurement cycle, the chamber humidity initially stabilized at 10% relative humidity (RH) for 5 min, followed by exposure to the target humidity level for another 5 min to measure the resistance response of the composite. Finally, the chamber was purged again at 10% RH for 10 min to complete a sensing cycle. All humidity-sensing experiments were conducted at room temperature, and the resistance responses were recorded using a Keithley 2400 source meter at a 1 V DC bias.

3. RESULT AND DISCUSSION

3.1 Dispersive Property Analysis of Montmorillonite/Graphene Composite

Figure 1 shows the crystal structure of MMT and its humidity absorption mechanism. MMT is a layered silicate consisting of tetrahedral $(SiO_4)^{4-}$ sheets and octahedral $Al(OH)_6$ sheets. The partial substitution of Si^{4+} by Al^{3+} in the tetrahedral sheets and Al^{3+} by Mg^{2+} in the octahedral sheets induces a net negative charge, which is compensated by exchangeable interlayer cations such as Na^+ and Ca^{2+}. These cations strongly attract polar water molecules, enabling MMT to intercalate water into its interlayer space and swelling to seven-fold along the z-axis [21,22].

Based on these properties, we fabricated an MMT/rGO composite for humidity-sensing applications, as shown in Fig. 2. The MMT suspension and graphene ink were mixed via sonication for 1 min to obtain a homogeneous MMT/rGO dispersion. Uniform dispersion of both components is essential for stable sensing performance [24]. The IPA solvent plays a crucial role in achieving uniformity. The graphene ink used in this study was dispersed in IPA because the polar hydroxyl group (–OH) of IPA can interact with oxygen functional groups on the rGO surface, preventing flake aggregation and stabilizing dispersion [25,26]. MMT also exhibits good dispersibility in IPA, as its interlayer cations (Na^+ and Ca^{2+}) interact with the –OH groups of IPA. Therefore, IPA effectively acts as a solvent to promote the homogeneous dispersion of both MMT and rGO flakes within the composite [27]. When the MMT/rGO dispersion is subjected to sonication, the electrostatic interactions between the oxygen functional groups on the rGO and the polar MMT layers further stabilize the mixture, preventing phase separation and yielding a well-dispersed composite solution. The resulting dispersion was spin-coated onto IDE-deposited glass substrates to obtain a uniform sensing layer, followed by

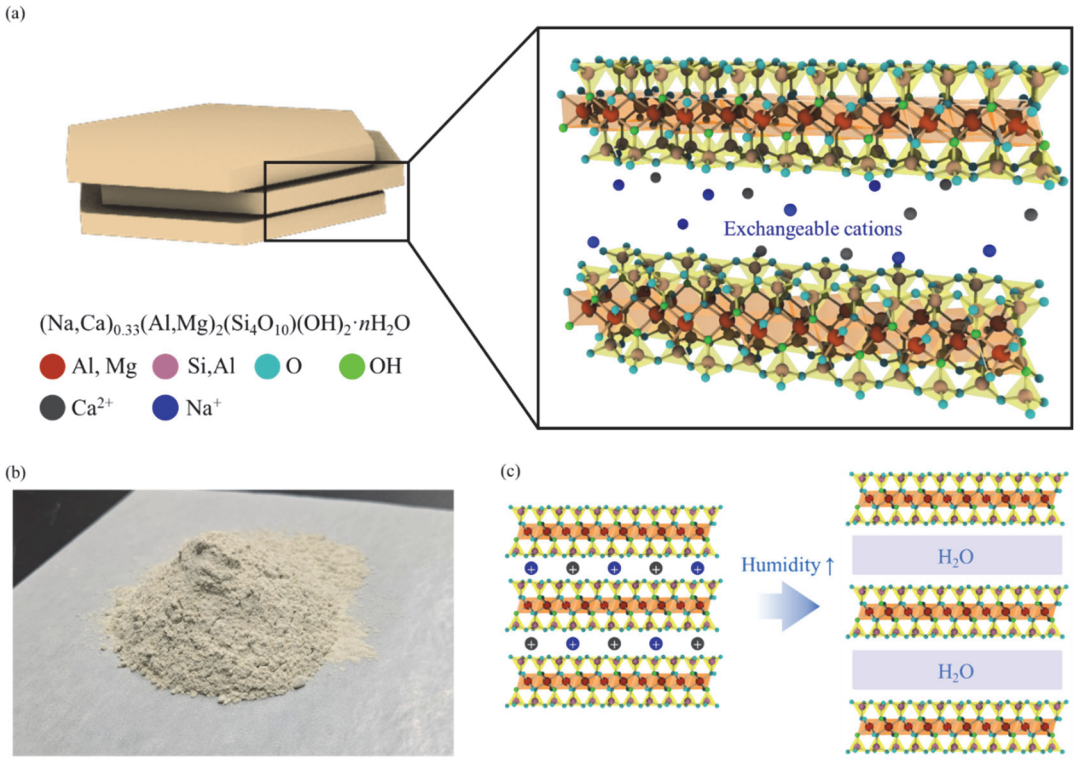

Fig. 1. (a) Schematic illustration of the layered structure of MMT, consisting of 2:1 tetrahedral–octahedral–tetrahedral sheets with interlayer cations, (b) optical image of the MMT powder, and (c) schematic depiction of the swelling mechanism of MMT, where interlayer Na^+/Ca^{2+} cations hydrate and expand the basal spacing upon water adsorption.

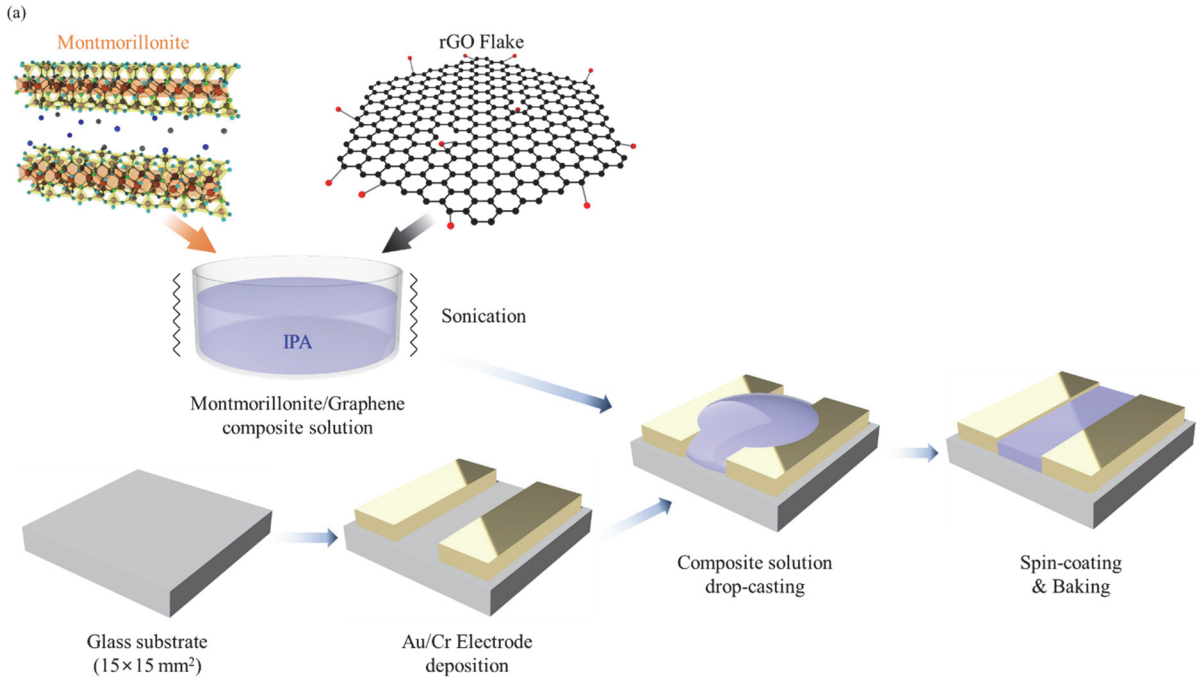

Fig. 2. (a) Schematic illustration of the fabrication process of the MMT/rGO composite resistive humidity sensor.

Table 1. Designation of MMT/rGO composite samples based on the volumetric mixing ratio of the MMT suspension to the rGO ink with the corresponding wt% of MMT and rGO in each composite formulation.

Sample	MMT (wt%)	rGO (wt%)
MGC-0	0	0.4
MGC-1	5.26	0.36
MGC-2	10.52	0.32
MGC-3	15.79	0.28
MGC-4	21.05	0.24
MGC-5	26.32	0.2
MGC-6	31.57	0.16
MGC-7	36.84	0.12

baking to complete the composite film formation. To investigate the effects of the composition on humidity-sensing performance, the mixing volume ratio between the MMT suspension and graphene ink was systematically varied from 0:10 to 7:3. Each composite was designated according to its MMT fraction, and the corresponding wt% of MMT and rGO for each composite formulation is summarized in Table 1.

The surface morphologies of the coating films were examined using FE-SEM, as shown in Figs. 3(a)–(c). The SEM image of the pure rGO sample shows overlapping two-dimensional flakes forming stacked lamellar structures [28], whereas the pure MMT film exhibits agglomerated clay-like platelets [29]. By contrast, the MMT/rGO composite displays rGO flakes uniformly embedded between the planar MMT layers, confirming a homogeneous dispersion without local aggregation. This morphology suggests that electrostatic coupling between rGO and MMT enables stable mixing during the solution process. EDS mapping was performed to qualitatively examine the distributions of MMT and rGO in the composite, as shown in Figs. 3(d)–(i). The characteristic elements of MMT (Mg, Al, Ca, and Na) [30] and carbon from rGO are evenly distributed throughout the image, further verifying the uniform distribution of the two phases. These observations confirm that the MMT/rGO composite fabricated via a simple solution-based process and brief sonication achieves excellent dispersion and structural homogeneity without phase segregation.

3.2 Humidity Sensing Response & Mixing Ratio Optimization

The humidity-sensing characteristics of the fabricated MMT/rGO composite sensors were evaluated by monitoring the resistance changes under controlled RH levels. The sensing mechanism is illustrated in Fig. 4(a). When conductive rGO flakes are incorporated into the insulating MMT, they form interconnected conductive networks that facilitate charge transport. Upon exposure to humid air, MMT intercalates water molecules within its interlayer region, causing expansion along the z-axis. This swelling disrupts the conductive pathways formed by the rGO flakes, thereby impeding electron transport and increasing overall resistance [1,24,31].

The humidity response varied with the MMT/rGO mixing ratio. The electrical percolation transition model describing this behavior is shown in Fig. 4(b) [31,32]. At low MMT contents, the rGO flakes readily formed continuous conductive networks, resulting in high electrical conductivity. As the MMT fraction increased, these networks gradually disconnected, and the overall conductivity decreased. When the MMT content approached the electrical percolation transition region, the composite exhibited a sharp increase in resistance due to the disruption of the conductive pathways. Once the MMT fraction exceeded the percolation threshold, most of the conductive paths collapsed, rendering the composite nearly insulating. Within this transition region, even minor structural perturbations, such as humidity-induced swelling, led to pronounced resistance modulation [24,33]. Therefore, identifying the optimal MMT/rGO composition within the electrical percolation transition region is essential for maximizing sensor sensitivity.

Figure 4(c) shows the resistances of the composites under different MMT/rGO ratios. Samples with low MMT fractions exhibited low resistance due to dominant conduction through the rGO networks. However, as the MMT fraction increased, the resistance sharply increased beyond the MGC-5 composition, indicating the onset of the percolation transition. Around MGC-6, the resistance increases abruptly, confirming that this ratio corresponds to the electrical percolation transition regime.

Figures 4(d) and 4(e) compare the humidity responses of composites with various MMT/rGO ratios under 50% RH

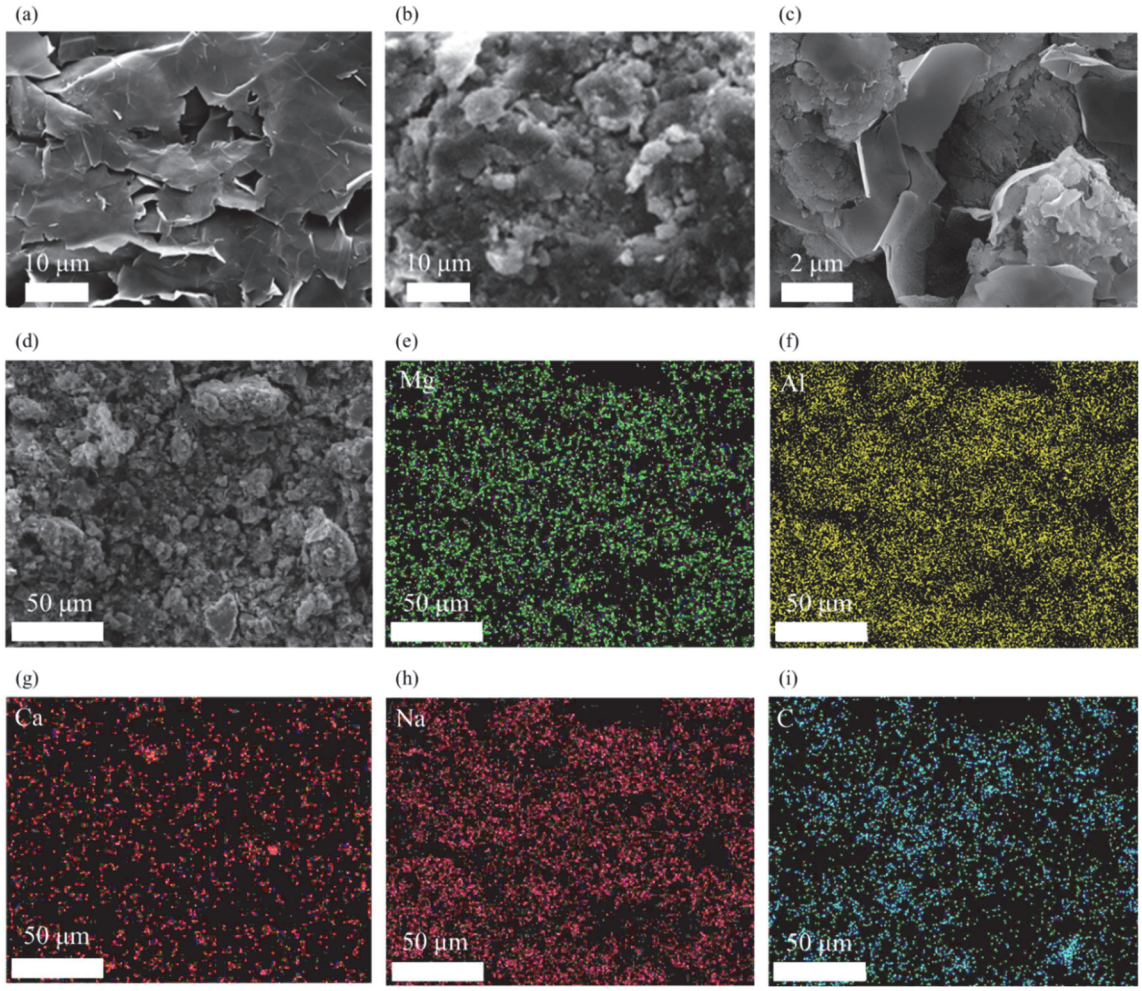

Fig. 3. SEM image of (a) pure rGO flake (10 kx) showing their overlapping two-dimensional flakes, (b) pure MMT (10 kx) displaying their agglomerated clay-like platelets, and (c) MMT/rGO composite (20 kx) with homogeneous dispersion. EDS elemental mapping of (d) MMT/rGO composite confirming the spatial distribution of major MMT components: (e) Mg, (f) Al, (g) Ca, (h) Na, and (i) the carbon signal corresponding to rGO.

(ΔRH = 40%). The responses were calculated using the following equations:

$$Response = \Delta R/R_0 \times 100\ (\%)$$

where R_0 is the baseline resistance at 10% RH, and ΔR is the resistance change at 50% RH.

Between the pure rGO film (MGC-0) and the low MMT composite (MGC-1), MGC-0 showed a larger humidity response of approximately 8%, whereas MGC-1 exhibited a lower response of 3%. This is because, at low MMT contents, the resistance variation is mainly dominated by the intrinsic moisture adsorption behavior of rGO rather than by MMT swelling. Therefore, MGC-1, which contained a smaller fraction of rGO flakes, exhibited a lower response to humidity. As the MMT fraction increased, the humidity response gradually increased, reaching a pronounced peak of 115% for MGC-6. This composition lies within the electrical percolation transition region identified in Fig. 4(c), where humidity-induced MMT swelling most effectively disrupts the rGO conductive pathways. Beyond this ratio, excessive MMT reduces the connectivity among the rGO flakes, leading to a decline in the humidity response despite increased water adsorption.

In addition to enhanced sensitivity, the dominant role of MMT in moisture adsorption also contributes to the superior

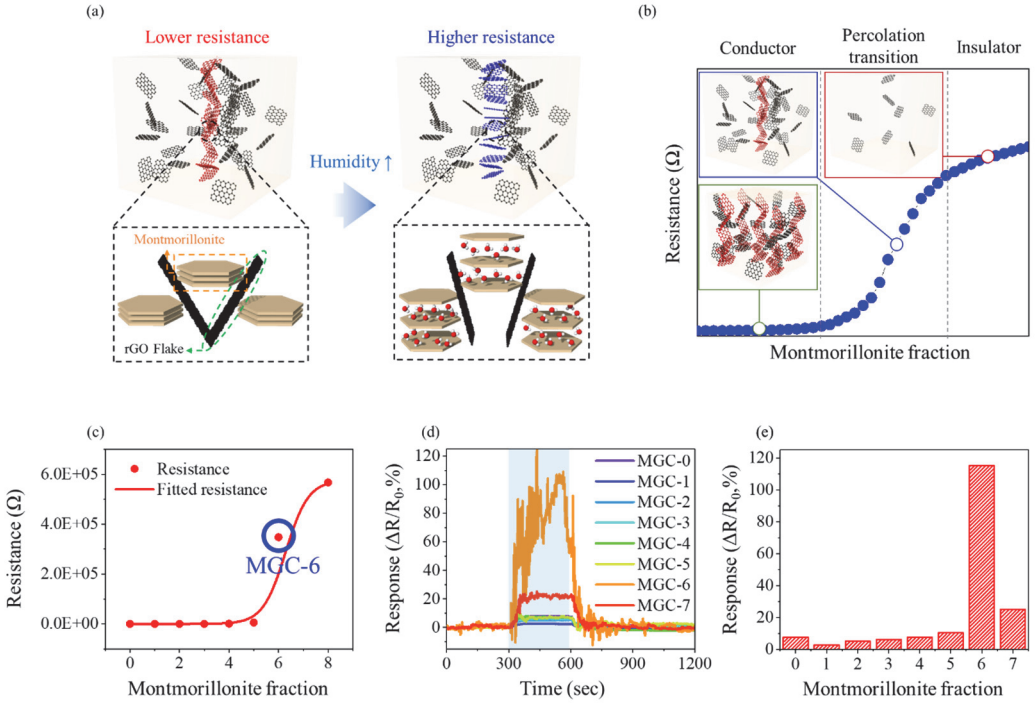

Fig. 4. (a) Schematic illustration of the humidity-sensing mechanism of the MMT/rGO composite, showing disruption of interconnected conductive networks consisted by rGO flakes under humid condition, (b) electrical percolation model depending on the MMT fraction in MMT/rGO composite, (c) variation in the measured electrical resistance of the MMT/rGO composite as a function of the MMT fraction, and (d), (e) humidity-sensing performance of the composite with different MMT fractions.

stability and repeatability of the composite sensor. Unlike rGO, which tends to form strong hydrogen bonds with water molecules, leading to irreversible adsorption and gradual oxidation by residual moisture [18], MMT exhibits a reversible humidity adsorption mechanism. The interlayer cations (Na^+ and Ca^{2+}) within MMT electrostatically interact with polar water molecules, allowing water to be absorbed and desorbed repeatedly without structural degradation. This reversible swelling–deswelling process enables the MMT layers to accommodate and release moisture dynamically, preventing the accumulation of trapped water on the rGO surface [21-23]. As a result, the MMT/rGO composite achieves not only high sensitivity but also outstanding long-term stability and reproducibility during cyclic humidity sensing.

Therefore, incorporating MMT into rGO flakes significantly enhances humidity sensitivity, with optimal performance achieved near the electrical percolation transition. In this regime, the synergistic interaction between the MMT swelling and rGO network modulation maximizes the resistance change of the sensor under varying humidity conditions.

4. CONCLUSION

In this study, an MMT/rGO composite was developed as a stable and biocompatible sensing material for resistive-type humidity detection. The composite was fabricated via a simple solution-based process using IPA as the solvent, which effectively promoted the homogeneous dispersion of MMT and rGO flakes. SEM and EDS analyses confirmed that both components were uniformly distributed without phase separation, demonstrating the reliability of the dispersion approach. The humidity-sensing characteristics revealed that MMT swelling under humid conditions modulated the conductive pathways formed by the rGO flakes, leading to distinct resistance variations. The humidity response strongly depended on the MMT/rGO mixing ratio, and the sensor exhibited the highest sensitivity near the electrical percolation transition region (MGC-6). These findings demonstrate that incorporating MMT into rGO matrices can effectively enhance humidity sensitivity at room temperature. Given its simple fabrication, cost-effectiveness, and high reversibility,

the proposed MMT/rGO composite is a promising candidate for wearable humidity sensors that can continuously and precisely monitor human respiration.

ORCID

Seoung-Ki Lee https://orcid.org/0000-0002-8786-0251

ACKNOWLEDGEMENTS

This work was financially supported by the Ministry of Trade, Industry & Energy of Korea (Grant No. 00269589 and 20019508).

REFERENCES

[1] S. Santra, G. Hu, R. Howe, A. De Luca, S. Ali, F. Udrea, J. Gardner, S. Ray, P. Guha, and T. Hasan, *Sci. Rep.*, **5**, 17374 (2015). doi: https://doi.org/10.1038/srep17374

[2] T. Liang, W. Hou, J. Ji, and Y. Huang, *Sens. Actuators A: Phys.*, **350**, 114104 (2023). doi: https://doi.org/10.1016/j.sna.2022.114104

[3] H. An, T. Habib, S. Shah, H. Gao, A. Patel, I. Echols, X. Zhao, M. Radovic, M. J. Green, and J. L. Lutkenhaus, *ACS Appl. Nano Mater.*, **2**, 948 (2019). doi: https://doi.org/10.1021/acsanm.8b02265

[4] Y. Luo, Y. Pei, X. Feng, H. Zhang, B. Lu, and L. Wang, *Mater. Lett.*, **260**, 126945 (2020). doi: https://doi.org/10.1016/j.matlet.2019.126945

[5] Y. Wang, L. Zhang, Z. Zhang, P. Sun, and H. Chen, *Langmuir*, **36**, 9443 (2020). doi: https://doi.org/10.1021/acs.langmuir.0c01315

[6] W. Noh, Y. Go, and H. An, *Sensors*, **23**, 1977 (2023). doi: https://doi.org/10.3390/s23041977

[7] H. Bi, K. Yin, X. Xie, J. Ji, S. Wan, L. Sun, M. Terrones, and M. S. Dresselhaus, *Sci. Rep.*, **3**, 2714 (2013). doi: https://doi.org/10.1038/srep02714

[8] C. Zhu, L. Q. Tao, Y. Wang, K. Zheng, J. Yu, X. Li, X. Chen, and Y. Huang, *Sens. Actuators B: Chem.*, **325**, 128790 (2020). doi: https://doi.org/10.1016/j.snb.2020.128790

[9] Y. Han, X. Kong, W. Wu, J. Li, X. Yang, Y. Guo, Y. Fu, H. Torun, X. Xiang, Y. Tang, and X. Zu, *Micro Nano Eng.*, **15**, 100127 (2022). doi: https://doi.org/10.1016/j.mne.2022.100127

[10] D. Zhang, R. Mao, X. Song, D. Wang, H. Zhang, H. Xia, Y. Ma, and Y. Gao, *Sens. Actuators B: Chem.*, **374**, 132824 (2023). doi: https://doi.org/10.1016/j.snb.2022.132824

[11] M. Shao, H. Sun, R. Zhang, L. Li, Y. Liu, and X. Qiao, *Opt. Fiber Technol.*, **68**, 102782 (2022). doi: https://doi.org/10.1016/j.yofte.2021.102782

[12] J. C. Yang, G. P. Kim, and K. T. Kim, *J. Korean Inst. Electr. Electron. Mater. Eng.*, **36**, 594 (2023). doi: https://doi.org/10.4313/JKEM.2023.36.6.9

[13] Z. Zhang, J. Huang, Q. Yuan, and B. Dong, *Nanoscale*, **6**, 9250 (2014). doi: https://doi.org/10.1039/C4NR01570C

[14] W. T. Koo, H. J. Cho, D. H. Kim, Y. H. Kim, H. Shin, R. M. Penner, and I. D. Kim, *ACS Nano*, **14**, 14284 (2020). doi: https://doi.org/10.1021/acsnano.0c05307

[15] S. Y. Park, J. E. Lee, Y. H. Kim, J. J. Kim, Y. S. Shim, S. Y. Kim, M. H. Lee, and H. W. Jang, *Sens. Actuators B: Chem.*, **258**, 775 (2018). doi: https://doi.org/10.1016/j.snb.2017.11.176

[16] J. Qian, R. Tan, M. Feng, W. Shen, D. Lv, and W. Song, *Chemosensors*, **12**, 230 (2024). doi: https://doi.org/10.3390/chemosensors12110230

[17] T. Xie, A. F. A. Rahman, A. A. Bakar, and A. Arsad, *J. Clust. Sci.*, **36**, 148 (2025). doi: https://doi.org/10.1007/s10876-025-02869-0

[18] C. Lv, C. Hu, J. Luo, S. Liu, Y. Qiao, Z. Zhang, J. Song, Y. Shi, J. Cai, and A. Watanabe, *Nanomaterials*, **9**, 422 (2019). doi: https://doi.org/10.3390/nano9030422

[19] C. Chen, X. Wang, M. Li, Y. Fan, and R. Sun, *Sens. Actuators B: Chem.*, **255**, 1569 (2018). doi: https://doi.org/10.1016/j.snb.2017.08.168

[20] J. W. An, H. J. Kim, and S. K. Lee, *J. Korean Inst. Electr. Electron. Mater. Eng.*, **36**, 203 (2023). doi: https://doi.org/10.4313/JKEM.2023.36.3.1

[21] I. E. S. Arruda, J. H. P. de Oliveira, B. P. G. de Lima Damasceno, M. F. de La Roca Soares, D. T. C. da Silva, and J. L. Soares-Sobrinho, *J. Nanopart. Res.*, **25**, 144 (2023). doi: https://doi.org/10.1007/s11051-023-05796-1

[22] M. Endo and H. Sato, *Minerals*, **14**, 430 (2024). doi: https://doi.org/10.3390/min14040430

[23] P. L. Hall and D. M. Astill, *Clays Clay Miner.*, **37**, 355 (1989). doi: https://doi.org/10.1346/CCMN.1989.0370409

[24] B. C. Serban, N. Dumbravescu, O. Buiu, M. Bumbac, C. Dumbravescu, M. Brezeanu, C. Pachiu, C. M. Nicolescu, C. Romanitan, and O. Brincoveanu, *Sensors*, **25**, 3047 (2025). doi: https://doi.org/10.3390/s25103047

[25] M. Ayán-Varela, J. Paredes, S. Villar-Rodil, R. Rozada, A. Martínez-Alonso, and J. Tascón, *Carbon*, **75**, 390 (2014). doi: https://doi.org/10.1016/j.carbon.2014.04.018

[26] S. Qamar, N. Ramzan, and W. Aleem, *Synth. Met.*, **307**, 117697 (2024). doi: https://doi.org/10.1016/j.synthmet.2024.117697

[27] D. Burgentzlé, J. Duchet, J. Gérard, A. Jupin, and B. Fillon, *J. Colloid Interface Sci.*, **278**, 26 (2004).
doi: https://doi.org/10.1016/j.jcis.2004.05.015

[28] S. W. Mushfiq and R. Afzalzadeh, *Sci. Rep.*, **12**, 9872 (2022).
doi: https://doi.org/10.1038/s41598-022-10971-W

[29] N. Suma, Y. Bhat, B. J. Prakash, and P. Iyengar, *Silicon*, **5**, 271 (2013).
doi: https://doi.org/10.1007/s12633-013-9151-5

[30] Z. Tu, Y. Chen, Y. Li, W. Zhang, and X. Cao, *Minerals*, **14**, 1077 (2024).
doi: https://doi.org/10.3390/min14111077

[31] K. P. Yoo, L. T. Lim, N. K. Min, M. J. Lee, C. J. Lee, and C. W. Park, *Sens. Actuators B: Chem.*, **145**, 120 (2010).
doi: https://doi.org/10.1016/j.snb.2009.11.041

[32] S. Barrau, P. Demont, A. Peigney, C. Laurent, and C. Lacabanne, *Macromolecules*, **36**, 5187 (2003).
doi: https://doi.org/10.1021/ma021263b

[33] B. C. Serban, C. Cobianu, N. Dumbravescu, O. Buiu, M. Bumbac, C. M. Nicolescu, C. Cobianu, M. Brezeanu, C. Pachiu, and M. Serbanescu, *Sensors*, **21**, 1435 (2021).
doi: https://doi.org/10.3390/s21041435